Diagn Interv Radiol 2016; 22:231–240

EXPERIMENTAL STUDIES

ORIGINAL ARTICLE

Perfusion parameters as potential imaging biomarkers for the early prediction of radiotherapy response in a rat tumor model

Ho Yun Lee
Namkug Kim
Jin Mo Goo
Eui Kyu Chie
Hye Jong Song

PURPOSE

We aimed to compare various tumor-related radiologic morphometric changes and computed tomography (CT) perfusion parameters before and after treatment, and to determine the optimal imaging assessment technique for the prediction of early response in a rat tumor model treated with radiotherapy.

METHODS

Among paired tumors of FN13762 murine breast cancer cells implanted bilaterally in the necks of eight Fischer rats, tumors on the right side were treated with a single 20 Gy dose of radiotherapy. Perfusion CT studies were performed on day 0 before radiotherapy, and on days 1 and 5 after radiotherapy. Variables based on the size, including the longest diameter, tumor area, and volume, were measured. Quantitative perfusion analysis was performed for the whole tumor volume and permeabilities and blood volumes (BVs) were obtained. The area under the curve (AUC) difference in the histograms of perfusion parameters and texture analyses of uniformity and entropy were quantified. Apoptotic cell density was measured on pathology specimens immediately after perfusion imaging on day 5.

RESULTS

On day 1 after radiotherapy, differences in size between the irradiated and nonirradiated tumors were not significant. In terms of percent changes in the uniformity of permeabilities between tumors before irradiation and on day 1 after radiotherapy, the changes were significantly higher in the irradiated tumors than in the nonirradiated tumors (0.085 [−0.417, 0.331] vs. −0.131 [−0.536, 0.261], respectively; $P = 0.042$). The differences in AUCs of the histogram of voxel-by-voxel vascular permeability and BV in tumors between day 0 and day 1 were significantly higher in treated tumors compared with the control group (permeability, 21.4 [−2.2, 37.5] vs. 9.5 [−8.9, 33.8], respectively, $P = 0.030$; BV, 52.9 [−6186.0, 419.2] vs. 11.9 [−198.3, 346.7], respectively, $P = 0.049$). Apoptotic cell density showed a significantly positive correlation with the AUC difference of BV, the percent change of uniformity in permeability and BV (r=0.202, r=0.644, and r=0.706, respectively).

CONCLUSION

By enabling earlier tumor response prediction than morphometric evaluation, the histogram analysis of CT perfusion parameters appears to have a potential in providing prognostic predictive information in an irradiated rat model.

From the Departments of Radiology and Center for Imaging Science (H.Y.L.) and Pathology (H.J.S.), Samsung Medical Center, Sungkyunkwan University School of Medicine, Seoul, Korea; the Department of Radiology and Research Institute of Radiology (N.K.), Asan Medical Center, University of Ulsan College of Medicine, Seoul, Korea; the Department of Radiology (J.M.G. ✉ *jmgoo@plaza.snu.ac.kr*), Institute of Radiation Medicine, and Cancer Research Institute, Seoul, Korea; the Department of Radiation Oncology (E.K.C.), Seoul National University College of Medicine, Seoul, Korea.

H. Y. Lee and N. Kim contributed equally to this work.

Received 15 May 2015; revision requested 6 July 2015; last revision received 14 October; accepted 22 October 2015.

Published online 29 March 2016.
DOI 10.5152/dir.2015.15171

With the advent of molecular biology, focus on drug development has shifted from cytotoxic chemotherapies to molecular targeted therapies. Many of these new therapies are expected to be primarily cytostatic in action, making traditional tumor size response criteria less appropriate for the early assessment of drug efficacy (1, 2). Thus, there is a need for development of noninvasive methods that are able to monitor tumor response to therapies while potentially providing a better assessment of the response of the whole tumor (3, 4).

One modality that requires continuous follow-up would be the field of radiotherapy. However, a substantial number of patients encounter treatment failure (5). A recent study showed that tumor response to radiotherapy is regulated by the degree of apoptosis in tumor endothelial cells; thus, tumor vasculature can be a powerful target for the treatment evaluation of radiotherapy (6). According to Ng et al. (7), the destruction of tumor vessels is related to radiation-induced tumor regression. Through the effects on oxygenation, tumor perfusion has a significant role in modulating radiotherapy response (8). Therefore, robust methods to evaluate the *in vivo* tumor vascular effects of radiotherapy are warranted.

Computed tomography (CT) perfusion has been developed as a noninvasive *in vivo* imaging method to investigate tumor-associated vasculature, and it is increasingly used to monitor treatment response and quantify tumor vascularity in various solid cancers (9–14). Its advantages include rapid scanning speed, high temporal and spatial resolution, and more importantly, routine availability; further, one of the greatest advantages of CT for perfusion imaging is the linear relationship between CT attenuation and iodine-based contrast concentration compared with other modalities, and this allows for an accurate absolute quantification of perfusion parameters (15).

CT perfusion analysis produces resulting parametric maps, for which each pixel represents a parameter value. Given significant tumor heterogeneity, a voxel-based approach may be more sensitive than the mean tumor averages of perfusion variables (16). The problem is that perfusion parameters to predict therapy response in the clinical setting might be more complex to quantify and compare due to the inherent pre- and post-treatment heterogeneities observed within tumors. Recently, Freiman et al. (17) developed a new approach to quantify the response of a tumor to therapy based on the entire cumulative histogram analysis. This method assesses the area under the curve (AUC) of a histogram curve, which is expressed as a particular parameter such as CT attenuation value or perfusion parameter, after the segmentation of tumor lesion, and then calculates the differences in AUCs of histogram curves in pre- and post-treatment. Therefore, their approach provides a single number that summarizes the overall tumor changes over time. Thus, it provides a potential solution to the problem of complexity.

Given the fact that the optimum measurement technique, appropriate response evaluation method, and magnitude of size change are subject to debate, we sought to compare various tumor-related radiologic morphometric changes and CT perfusion parameters before and after treatment, and to determine the optimal imaging assessment technique for the prediction of early response in a rat tumor model treated with radiotherapy. To this end, we conducted response measurements according to size and perfusion parameters (mean value, CT texture, and value based on the entire cumulative histogram analysis).

Main points

- To predict early radiotherapy response in a rat tumor model, we compared various tumor-related radiologic morphometric changes and CT perfusion parameters.
- When compared between before and one day after irradiation, change in uniformity of permeability value of irradiated tumors was significantly higher than that of nonirradiated tumors.
- Apoptotic cell density showed a significant positive correlation with the AUC difference of blood volume, the percent change of uniformity in permeability, and the blood volume one day after irradiation.
- There was a significant positive correlation between the percent change of uniformity and the AUC difference in the permeability value.

Methods

Animal preparation

We used 10 female Fischer 344 rats (Charles River, Sulzbach) weighing between 200 g and 240 g and the FN13762 murine mammary carcinoma cell line (18) (American Type Culture Collection; Manassas) as an experimental animal tumor model. The study protocol was reviewed and approved by the Animal Care and Use Committee of our institute.

The methods for the animal tumor model were described in detail in a previous report (19). For subcutaneous tumor cell implantation, anesthesia was induced with a mixture of isoflurane (Isoflurane Belamont, Belamont Laboratories) and medical oxygen (isoflurane 5%; medical oxygen, 3 L/min) produced by an anesthetic gas evaporator (Minerve, Esternay). Anesthesia was maintained with an intramuscular injection of 10 mg/kg of ketamine hydrochloride (Ketalar; Yuhan Yanghang) and 4 mg/kg of xylazine hydrochloride (Rompun, Bayer Korea). FN13762 cells were inoculated bilaterally into the subcutaneous layer of the posterior neck of the rats with a 24-gauge needle by injecting 5×10^6 cells suspended in 0.1 mL of Dulbecco's modified Eagle's medium (Cambrex Biosciences, Verviers). Cellular viability was tested prior to tumor implantation using trypan blue; this always yielded a result of >90%. All procedures were performed using an aseptic technique. Animals were monitored through the recovery period and were returned to their cages. Tumor growth was checked with ultrasonography and electronic calipers daily following tumor implantation.

Perfusion CT

The tumors were allowed to grow up to 15 mm in diameter using ultrasound, which typically required seven days, before irradiation. When the tumors grew to approximately 15 mm in diameter, a perfusion CT examination of them was performed. Anesthesia for CT scanning was induced and maintained with an intramuscular injection of 4 mg/kg of xylazine hydrochloride and 10 mg/kg of ketamine hydrochloride. The tail vein was catheterized with a 24-gauge plastic cannula (Ethicon, Johnson & Johnson Medical) for contrast material injection. Each rat was placed and fixed in a plastic frame where the posture of rats could be maintained throughout the study.

CT scans were acquired during shallow self-breathing. Perfusion CT scanning was performed using a 64-slice scanner (Somatom Definition, Siemens Medical Solutions) with a 512×512 pixel matrix, 120 kV, 80 mAs, 14×1.2 mm collimation, 5–8 mm table feed/rotation, and 0.5 s rotation time. An initial unenhanced study was performed to cover the entire tumor. A bolus of contrast material (iopromide, Ultravist 370, Schering) was administered using an in-house dual injector with a micropump. The bolus infusion was administered at a decreasing rate (0.32 mL at 0.02 mL/s for 16 s, 0.16 mL at 0.01 mL/s for 16 s, and 0.28 mL at 0.007 mL/s for 40 s) and was followed by a saline flush (0.1 mL at 0.01 mL/s for 10 s). The infusion protocol was adopted from that of Ng et al. (20) and was modified for a small animal. Regarding Patlak analysis, contrast concentration of the tissue was equivalent to the sum of the intravascular and extravascular contrast concentrations at any time point, as denoted by the following equation:

$$C_t = rbv \times b_t + K \times \int b_t \times dt,$$

where C_t is the concentration of contrast material within the tissue, rbv is the relative blood volume of the tissue, b_t is the concentration of contrast material in the blood, and K is the permeability. By plotting this graphically, the permeability can be derived from the gradient of the slope of this line, and relative blood volume (BV) can be derived from the y-intercept (Fig. 1). Perfusion CT study was repeated on days 1 and 5 after irradiation to the right-side tumor (21).

Irradiation

X-ray irradiation was delivered with a Clinac 4/100 (Varian Medical Systems), with 4 MV, field size of 5×5 cm^2, effective field size of 4×4 cm^2, dose rate of 280 MU/min,

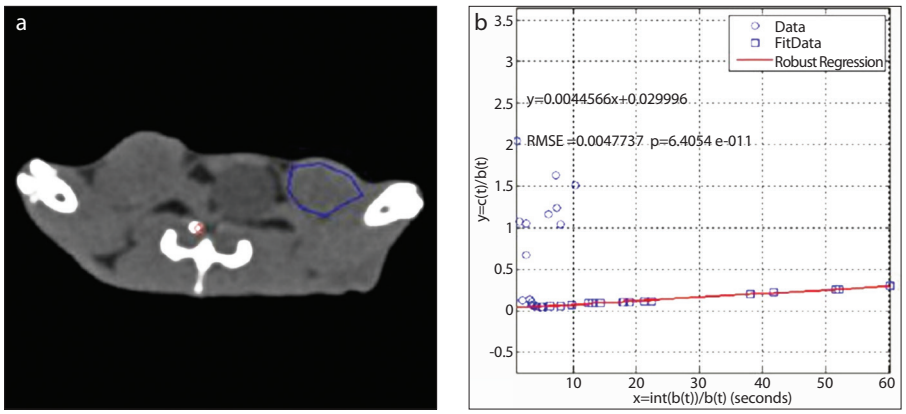

Figure 1. a, b. Patlak plot for the study. The graph shows representative fits of the Patlak model **(a)**. The x-axis represents time (s) and y-axis represents compartmental volume (mL). Permeability is derived from the gradient of slope and blood volume from the y-intercept **(b)**.

source to-surface distance of 100 cm, and depth of 2 cm. The tumor on the right side of the neck was chosen and exposed to a single dose of x-rays of 20 Gy, with the left tumor and the remainder of the rat torso shielded with a 4 mm thick lead shield. The left nonirradiated tumor served as a control.

Image processing and analysis

Data were transferred to a workstation (Leonardo, Siemens Medical Solutions). Among the 10 rats, two were excluded from the analysis because of unwanted death during anesthesia for the pretreatment CT scan. Therefore, there were images from 24 perfusion studies for evaluation (eight rats, three series each). CT scans were jointly assessed by one chest radiologist (nine years of experience in CT interpretation) and one radiology physicist (13 years of experience in radiology physics). Variables based on the size of each lesion were assessed in terms of the longest diameter, tumor area, and tumor volume using a semi-automated software tool (Syngo CT Oncology, Siemens Medical Solutions). On the same workstation, a region of interest (ROI) covering as large an area as possible of the whole tumor was drawn. ROI was drawn freehand around the tumor using an electronic cursor and mouse.

CT perfusion parameters were analyzed using an in-house software (MIL, Seoul) based on the Interactive Data Language (ITT Visual Solutions). The arterial input was determined from bolus-tracking images for the tumor side of each rat, and ROIs of the whole tumor drawn above were used; the software substantially calculated permeability and BV using Patlak analysis automatically (22).

The area under the curve (AUC) difference in the histogram of perfusion parameters was quantified using the following steps: for the permeability and BV maps of each tumor, ROI, and time point, a normalized cumulative histogram was computed (Fig. 2). Next, the differences between the histograms over time (before irradiation – on day 1 after irradiation; before irradiation – on day 5 after irradiation) were computed for both the irradiated and nonirradiated tumor ROIs (Fig. 2k). Finally, AUC was computed for each difference histogram, where the histogram AUC of the tumor (T) was normalized by the histogram AUC of the nontumorous soft tissue (NT) [$dNT/dT_{Normalized} = (dH/dTt)/(dH/dT_{nt})$]. The resulting measurement provides a single number that summarizes the entire changes in the permeability or BV (Fig. 2).

Heterogeneity within this ROI was also quantified by calculating entropy (irregularity, *e*) and uniformity (distribution of gray level, *u*) (23) with the following equations:

$$e = -\sum_{I=1}^{k} [P(I)] \log_2 [P(I)]$$

and

$$u = \sum_{I=1}^{k} [P(I)]^2$$

where *I* is the pixel value [between *I*=1 to *k* (where k is the highest pixel value)] in ROI and P (*I*) is the probability of the occurrence of that pixel value. Higher entropy and lower uniformity represent increased heterogeneity (24). We did not apply any filtration step because there are no establishments that enable the confirmation or refute the supposition for filtered texture data yet.

All approaches for quantitative response measurement are summarized in Fig. 3.

Histologic analysis

After CT imaging on day 5 after irradiation, the rats were euthanized with an overdose of ketamine and xylazine, and tumors were excised and dissected. Each resection specimen was evaluated with standard pathologic methods as described in the surgical pathology dissection manual of the Department of Pathology (25). For tumor sampling, a tumor tissue of approximately 10 mm in diameter per slide was obtained. With a hematoxylin–eosin stain, terminal deoxynucleotidyl transferase-mediated dUTP nick end labeling (TUNEL) staining of each tumor tissue was performed. With regard to the details of the tumor tissue staining procedure, the methods used by Kim et al. (26) were adopted. Three digital pictures were taken (original magnification, ×250), away from the areas of necrosis but otherwise randomly, for each tumor slice that had undergone TUNEL staining by a pathologist (six years of experience in histologic studies) who was blinded to the treatments that each animal received. A camera (SPOT) on a microscope (Nikon Optiphot 2; Nikon) interfaced with a personal computer and SPOT software was used to image the stained slides. These images were analyzed using noncommercial software from the National Institutes of Health (ImageJ, version 1.37v; National Institutes of Health). Apoptotic (TUNEL-stained) cells were segmented according to the signal intensity difference between target cells and background in each picture, while the intensity and minimum particle size thresholds were manually determined, and cell number was then counted in all three pictures per tumor. The total cell number in the three pictures was also counted with the same procedure, and the cell density (target cell number divided by the total cell number) was calculated (Fig. 4). For the count of apoptosis, total tumor cells were considered. Uneven background intensity was corrected by using the "rolling ball" algorithm (27), while the radius was manually determined.

Statistical analysis

The descriptive analysis was expressed in terms of mean and standard deviations when data is normally distributed and in terms of median with minimum and maximum when data is not normally distributed. The nonparametric Wilcoxon signed-rank test was used to compare each variable between the irradiated right-side and nonirradiated left-side tumors. Interrelationships

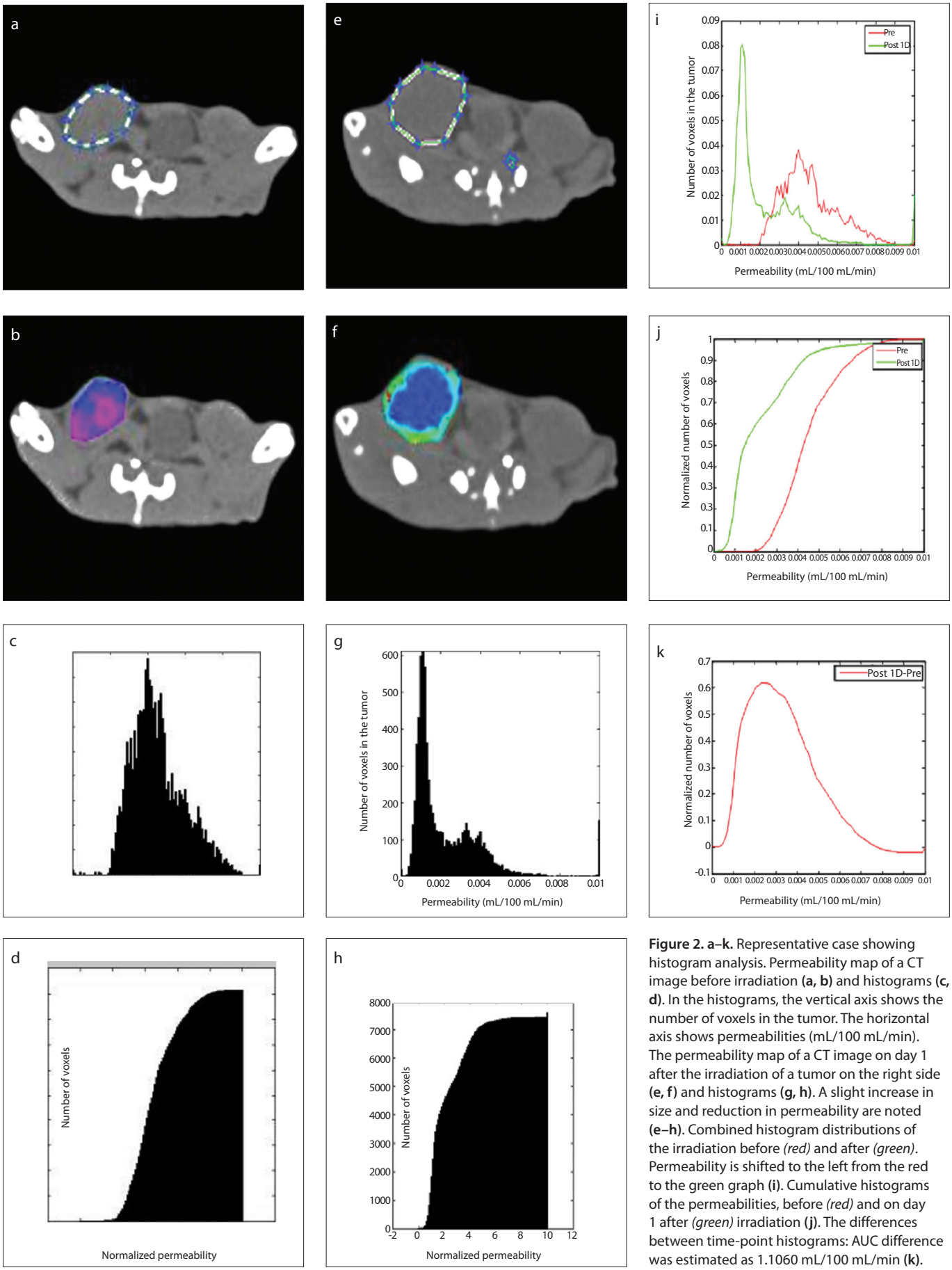

Figure 2. a–k. Representative case showing histogram analysis. Permeability map of a CT image before irradiation **(a, b)** and histograms **(c, d)**. In the histograms, the vertical axis shows the number of voxels in the tumor. The horizontal axis shows permeabilities (mL/100 mL/min). The permeability map of a CT image on day 1 after the irradiation of a tumor on the right side **(e, f)** and histograms **(g, h)**. A slight increase in size and reduction in permeability are noted **(e–h)**. Combined histogram distributions of the irradiation before *(red)* and after *(green)*. Permeability is shifted to the left from the red to the green graph **(i)**. Cumulative histograms of the permeabilities, before *(red)* and on day 1 after *(green)* irradiation **(j)**. The differences between time-point histograms: AUC difference was estimated as 1.1060 mL/100 mL/min **(k)**.

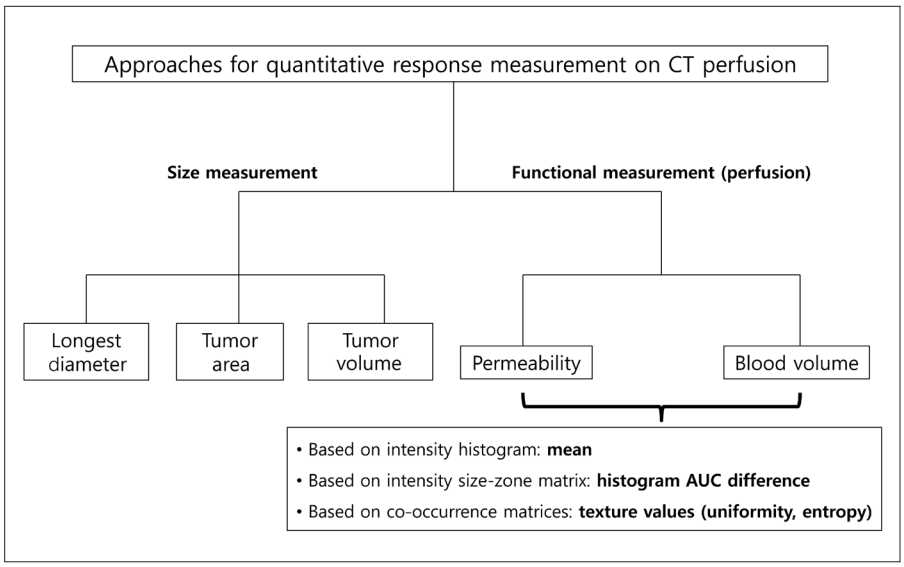

Figure 3. Diagrams illustrate all approaches for the quantitative response measurement.

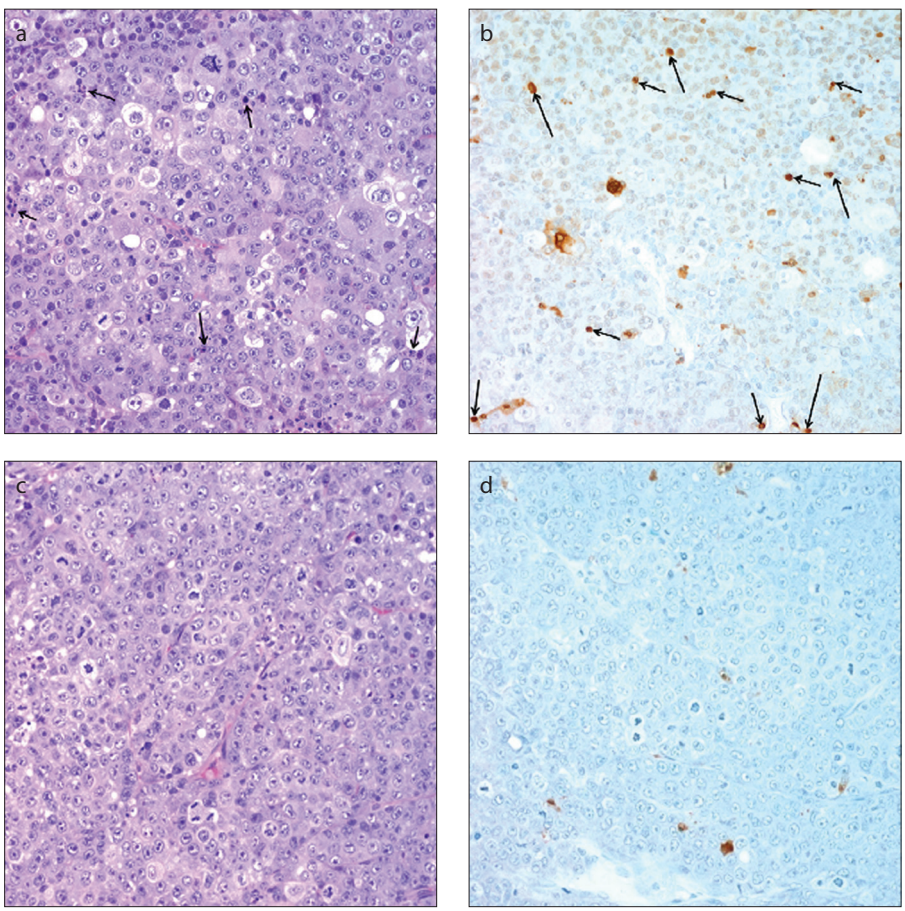

Figure 4. a–d. Histologic analysis of tumor response. Representative hematoxylin-eosin (HE)-stained **(a)** and terminal deoxynucleotidyl transferase-mediated dUTP nick end-labeling (TUNEL)-stained **(b)** slices of the tumor collected on day 5 after irradiation (original magnification, ×250). Apoptotic cells are indicated by *arrows*. Apoptotic cell density was estimated to be 0.86% (total cell count using image J, 1272; TUNEL-positive nuclei count, 11). HE-stained **(c)** and TUNEL-stained **(d)** slices of the nonirradiated tumor. There are no TUNEL-positive nuclei in this field.

between imaging parameters and pathologic response (apoptotic cell density) were assessed using the Spearman correlation coefficient test. For the sequential change of heterogeneity parameters, linear by linear association in the chi-square test was used to verify the existence of a time-related trend.

Statistical analyses were performed with SPSS software (SPSS version 19.0, IBM Corp.). A P value of <0.05 was considered to indicate a significant difference.

Results

All CT measurements, including CT perfusion parameters for nonirradiated and all irradiated tumor groups, are summarized in Fig. 5.

No statistically significant differences between the irradiated and nonirradiated tumors were noted in terms of size measurement or perfusion parameters. In the nonirradiated tumors, the mean values of size measurements and permeability were elevated, and those of BV were consistently reduced on both days 1 and 5. In the irradiated tumors, sizes were slightly elevated on day 1 after irradiation, but reduced on day 5. BV decreased on day 1, but was slightly elevated on day 5. Permeability consistently increased, and these changes by irradiation were more likely than those in the nonirradiated tumors.

Differences in size measurements between the irradiated and nonirradiated tumors were not significant on day 1 after irradiation, whereas the median sizes in irradiated tumors were significantly smaller than those in the nonirradiated tumors on day 5 (diameter, $P = 0.009$; tumor area, $P < 0.001$; tumor volume, $P < 0.001$). No significant difference was observed in other variables between the irradiated and nonirradiated tumors on day 1 and even on day 5.

In terms of the heterogeneity of tumor perfusion parameters, entropy decreased and uniformity consistently increased both on days 1 and 5 after irradiation in the permeability and BV of the irradiated tumors. These time-related trends were statistically significant (entropies of permeability and BV, $P = 0.029$ and $P = 0.013$, respectively; uniformities of permeability and BV, $P = 0.034$ and $P = 0.028$, respectively). On the other hand, the nonirradiated tumors showed more heterogeneous changes on day 1. Five days after, even the control group became more homogeneous probably due to a significant necrotic change.

In terms of percent change before and on day 1 after irradiation (Table 1, Fig. 6), the change in the uniformity of permeability of irradiated tumors was significantly higher than that of the nonirradiated tumors ($P = 0.042$). Further, significant increases in the

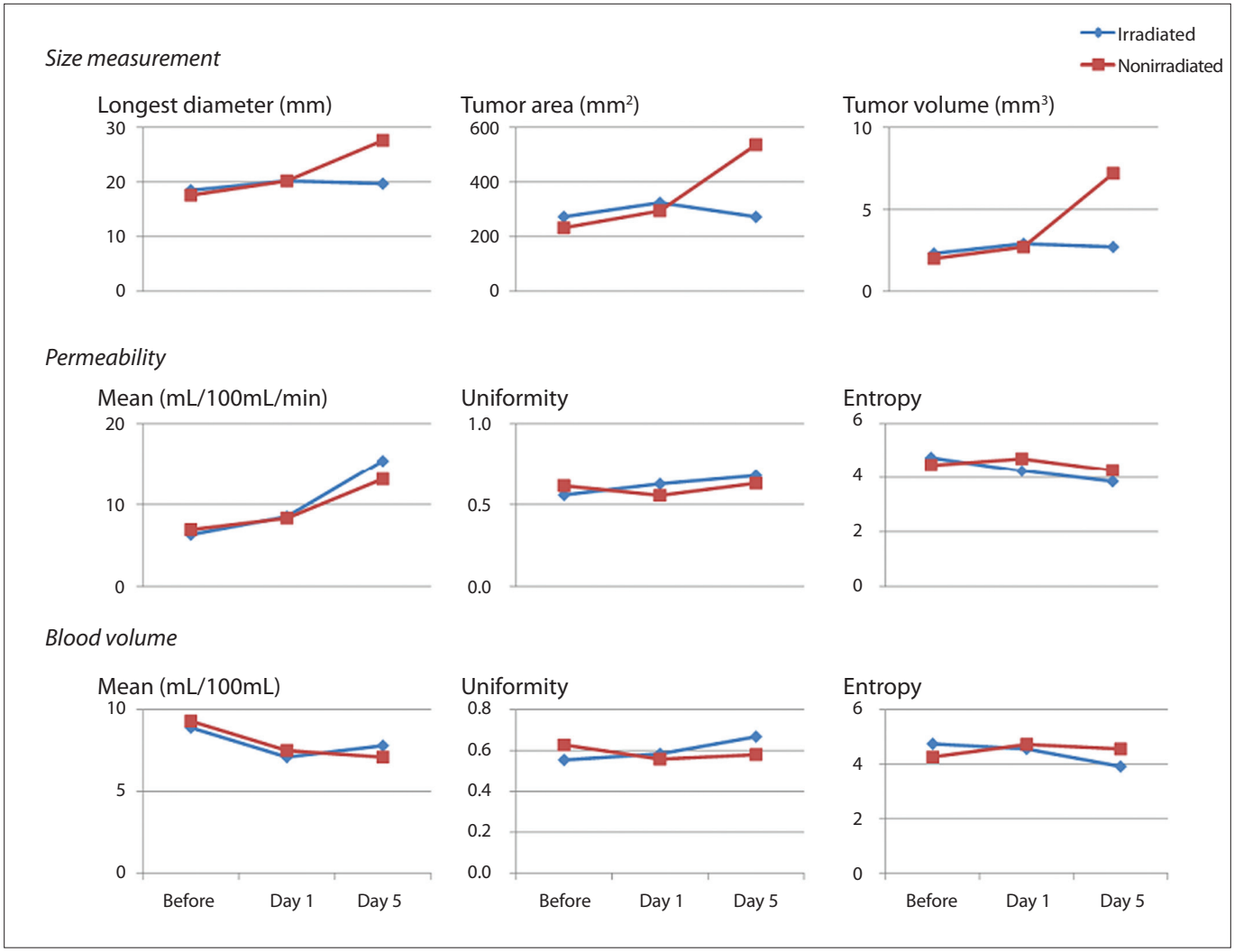

Figure 5. CT measurements. Differences in size measurements between the irradiated and nonirradiated tumors were not significant on day 1 after irradiation. The median values of size measurements in the irradiated tumors were significantly smaller than those in the nonirradiated tumors on day 5 (all $P < 0.01$). No significant difference was observed in other variables between the irradiated and nonirradiated tumors on day 1 or day 5. However, tumor entropy decreased and uniformity sequentially increased on days 1 and 5 both in permeability and blood volume of the irradiated tumors. This trend was statistically significant (all $P < 0.05$).

histogram AUC difference of vascular permeability and BV were observed after irradiation compared with those in the control group ($P = 0.030$ and $P = 0.049$, respectively).

The apoptotic cell density in the irradiated tumor group was 0.75% (0.39%, 1.26%) and significantly higher than that in control group (0.05% [0%, 0.16%]) ($P = 0.005$).

The apoptotic cell density showed a significant positive correlation with the AUC difference of BV, the percent change of uniformity in permeability, and BV on day 1 after irradiation (r = 0.202, $P = 0.035$; r = 0.644, $P = 0.024$; and r = 0.202, $P = 0.004$; respectively). However, there was no significant interrelationship between other CT parameters on day 1 and apoptotic cell density (Table 2).

Table 3 shows a significant positive correlation between the percent change of uniformity and the AUC difference in the permeability (r = 0.515, $P = 0.023$).

Discussion

In this study, we established a small animal model for Patlak analysis and determined the feasibility of a new quantitative analysis method (histogram difference) for treatment response evaluation using a multiparametric approach on the whole tumor basis.

At first, our results highlighted the challenges in obtaining an accurate representation of the perfusion curve of the Patlak model. Patlak analysis is a two-compartment model with one-way transfer of contrast material from the intravascular compartment to the extravascular extracellular compartment and allows BV and permeability to be determined. This method is a more straightforward approach to quantification than the distributed parameter model (28). In addition, it has an advantage over the distributed parameter model in that a high temporal resolution acquisition protocol is not necessary. Therefore, the assessment of tumor volume coverage can be greater, allowing whole tumor analysis to be performed (29). However, even for patients, a detailed contrast material infusion protocol is necessary, and further, a substantial infusion time is required, which is why there has been no animal tumor model for Patlak analysis. We obtained a Patlak plot on our rat tumor model with CT perfusion using a micropump system.

Regarding the interaction between ionizing radiation and tumor vasculature, one study has shown that tumor response to

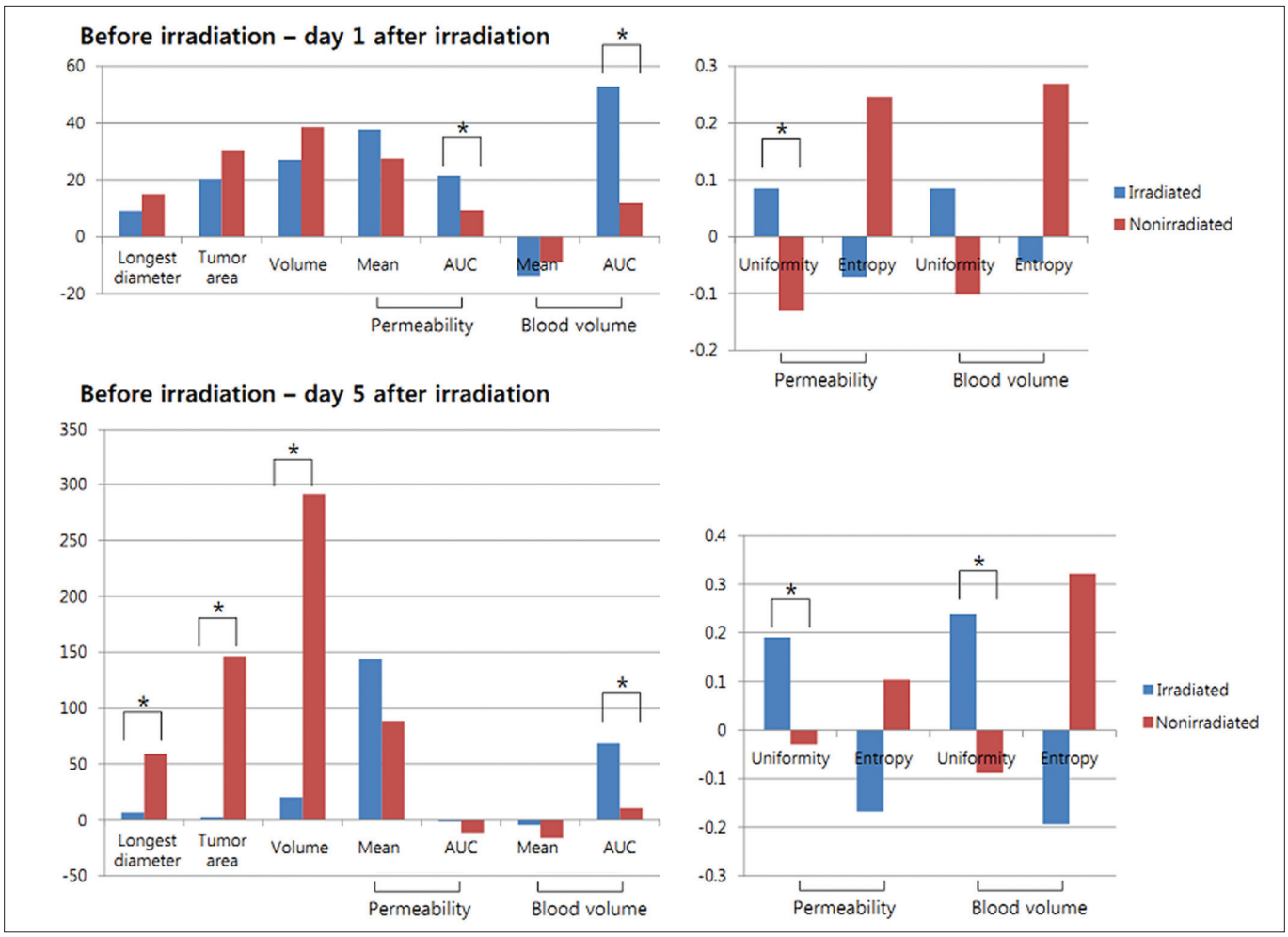

Figure 6. Changes in CT parameters. In terms of percent change before irradiation and day 1 after irradiation, change in the uniformity of the permeability of the irradiated tumors was significantly higher than that of the nonirradiated tumors ($P = 0.042$). Further, significant increases in the histogram AUC difference of vascular permeability and blood volume were observed after irradiation compared with those in the control group ($P = 0.030$ and $P = 0.049$, respectively). Refer to Table 1 for the scale of the y-axis for each parameter.

radiation may be regulated by tumor endothelial cell apoptosis (6). In addition, the upregulation of vascular endothelial growth factor reported in various cancer types after ionizing radiation may bring about increased perfusion and neovascularization (30). A recent study on lung cancer patients showed increased perfusion after radiation (7). In this study, the mean tumor permeability increased in both irradiated and nonirradiated tumors, whereas the mean tumor vascular BV decreased in both. Moreover, the difference in perfusion parameters between the irradiated and nonirradiated tumors was not significant in terms of the median value for day 1 and even for day 5 after irradiation. A similar phenomenon was observed in a recent study by Galban et al (16), where perfusion magnetic resonance imaging (MRI) was evaluated as a potential biomarker for response monitoring. They observed quantitative alterations in relative cerebral BV and flow maps during treatment. However, the average value of the mean tumor perfusion during treatment was found to lack sufficient sensitivity to accurately evaluate treatment outcome. These results were probably due to the heterogeneous changes in BV or flow occurring throughout the tumor, which ultimately desensitizes the whole tumor measurement.

In comparison, through voxel-by-voxel analysis using the parametric response map (PRM), spatial information could be preserved and local variations in terms of tumor PRM voxels after therapy initiation could be delineated from each other and therefore visualized and quantified within the context of the anatomical image. The problem is that this approach suggested by Galban et al. (16) is not technically applicable in all solid tumors. For voxel-by-voxel analysis between pre- and post-treatment maps, an unchanged outline of the tumor may be ideal or, if not, complex postprocessing including nonrigid registration is a prerequisite to voxel-by-voxel analysis. Furthermore, optimal registration might fail in cases of a significant change of regional anatomical structures or significant change of voxel number.

In view of this, our method using the histogram AUC difference was a more sensitive technique for the quantification of treatment-induced early alterations in perfusion parameters. A change in the number of voxels is not an issue because this analysis goes through normalization and cumulation. This measure summarizes the entire tumor response, including tumor heterogeneity, without prior image nonrigid registration, which is susceptible to inherit a registration error. Further, this method is simple and intuitive to interpret, unlike existing methods that solely use the difference between tumor ROI median/mean values, and it provides a single

Table 1. Percent changes in CT parameters

	Before irradiation – day 1			Before irradiation – day 5		
	Irradiated	Nonirradiated	*P*	Irradiated	Nonirradiated	*P*
Size measurements						
Longest diameter (mm)	9.2 (5.7, 18.9)	15.0 (8.8, 25.8)	0.273	6.8 (–3.6, 14.4)	59.1 (39.0, 82.6)	0.012
Tumor area (mm^2)	20.3 (8.8, 27.3)	30.5 (8.1, 51.5)	0.403	2.9 (–23.3, 17.5)	146.2 (50.6, 201.2)	0.013
Tumor volume (mm^3)	27.1 (24.0, 26.2)	38.6 (11.9, 56.9)	0.274	20.3 (5.2, 32.0)	291.2 (158.4, 428.0)	0.013
Permeability						
Mean (mL/100 mL/min)	37.8 (–8.4, 120.6)	27.5 (–12.1, 83.4)	0.311	143.9 (–44.0, 363.9)	88.4 (7.6, 178.4)	0.302
Histogram AUC difference	21.4 (–2.2, 37.5)	9.5 (–8.9, 33.8)	0.030	–1.4 (–67.9, 26.9)	–11.3 (–78.8, 25.2)	0.039
Uniformity	0.085 (–0.417, 0.331)	–0.131 (–0.536, 0.261)	0.042	0.191 (0.014, 0. 430)	–0.030 (–0.268, 0.315)	0.019
Entropy	–0.071 (–0.480, 0. 133)	0.246 (–0.319, 0.887)	0.124	–0.168 (–1.490, 0.260)	0.103 (–0.419, 0.557)	0.087
Blood volume						
Mean (mL/100 mL)	–13.7 (–66.7, 48.0)	–9.0 (–69.7, 32.0)	0.650	–4.7 (–48.5, 38.6)	–16.1 (–54.8, 17.3)	0.338
Histogram AUC difference	52.9 (–6186.0, 419.2)	11.9 (–198.3, 346.7)	0.049	68.5 (–33.9, 202.6)	10.5 (–103.0, 161.5)	0.007
Uniformity	0.085 (–0.155, 0.283)	–0.102 (–0.263, 0.310)	0.085	0.238 (–0.211, 0.541)	–0.089 (–0.302, 0.424)	0.004
Entropy	–0.044 (–0.386, 0.144)	0.269 (–0.283, 0.594)	0.201	–0.193 (–0.489, 0.144)	0.322 (–0.920, 0.571)	0.094

Data are expressed as median (minimum, maximum).
CT, computed tomography; AUC, area under the curve.

Table 2. Correlation of imaging biomarker with pathologic apoptotic cell density

Change in parameters (before irradiation – day 1 after irradiation)	r	*P*
Size measurement		
Longest diameter (mm)	–0.387	0.055
Tumor area (mm^2)	–0.129	0.310
Tumor volume (mm^3)	–0.301	0.063
Permeability		
Mean (mL/100 mL/min)	–0.344	0.080
Uniformity	0.644	0.024
Entropy	–0.387	0.094
Histogram AUC difference	0.460	0.077
Blood volume		
Mean (mL/100 mL)	–0.239	0.179
Uniformity	0.706	0.004
Entropy	–0.607	0.052
Histogram AUC difference	0.202	0.035

AUC, area under the curve.

number that summarizes the overall tumor perfusion changes over time (Table 4).

Assuming that a broad coverage of a tumor will be more representative for heterogeneous tumors, we measured CT perfusion parameters in the whole tumor volume. Ng et al. (7) observed different perfusion between the tumor rim and center after radiotherapy. Heterogeneous vascular changes between the tumor rim and center may be explained by the uneven distribution of vascularization and vasodilation and neovessel formation effects caused by radiation. Reiner et al. (31) compared perfusion parameters obtained from three-dimensional volumes-of-interest (3D-VOIs) with those obtained from a two-dimensional (2D)-ROI covering the lesion. Comparisons revealed considerable differences in blood flow, BV, and flow extraction product among 3D-VOI and 2D-ROI measurements in up to 68% of tumors. Thus, the functional assessment of tumor vascularization should aim at a broad coverage in the z-axis to allow for the reliable and accurate quantification of perfusion of the tumor as a whole.

In our study, the tumor vessel permeability did not change in the same direction with BV. In other words, permeability increased when BV decreased in the irradiated tumors. According to one study, changes in permeability are more spatially dependent than changes in BV (7). There were no significant changes in permeability after the sixth fraction of radiotherapy, for which the authors provided the establishment of equilibrium between vessel permeability and interstitial pressure as the reason. Changes in tumor vascularity may be dose-dependent and vary according to fraction size. Effects of radiation to tumor vascularity may also influence the radiosensitivity of tumors as well as normal tissues. Tumor perfusion measured with dynamic contrast-enhanced MRI showed significant increases in the first and second week of preoperative chemoradiotherapy in patients with rectal cancer (32). In contrast, in another rectal cancer study, significant decreases in blood flow were observed after preoperative chemoradiotherapy (33). A better understanding of changes in tumor vascularity after radiation through *in vivo*

Table 3. Correlation of AUC differences with heterogeneity variables on CT perfusion parameters (before irradiation – day 1 after irradiation)

CT perfusion	Uniformity change (%)		Entropy change (%)	
Permeability				
Histogram AUC difference	0.515	0.025	−0.406	0.079
Blood volume				
Histogram AUC difference	0.285	0.283	−0.297	0.258

CT, computed tomography; AUC, area under the curve.

Table 4. Recent quantitative analysis techniques for tumor response evaluation

	Parametric response map	Texture analysis	Histogram AUC difference
Based on	Co-occurrence matrices	Co-occurrence matrices	Intensity size-zone matrix
Pros	Voxel-by-voxel analysis sensitive to local variation	Reflects tumor heterogeneity	Difference in the number of voxels is not an issue; No problem on variability regarding filtering; Represented as a single number
Cons	Registration	Too many parameters Filtering issue	Not yet established

AUC, area under the curve.

monitoring is clinically relevant. In particular, the most radical radiotherapy has recently been combined with chemotherapy; novel radiation schedules are also being developed incorporating new agents such as vascular targeting drugs or monoclonal antibodies. Thus, a better understanding of changes in tumor vasculature after radiotherapy may better guide the timing of chemotherapy and even novel drugs.

The assessment of tumor heterogeneity on imaging is a recent issue. Heterogeneity, such as that of the tumor blood supply, is a well-recognized characteristic of malignancy. Goh et al. (23) assessed changes in the CT texture of tumors in patients with metastatic renal cell cancer treated with tyrosine kinase inhibitors (TKIs). They observed that CT entropy decreases and uniformity increases with TKIs, reflecting a decrease in tumor heterogeneity. In their study, texture analysis was performed for a limited tumor area and not for the whole tumor and should also be validated through various CT protocols. We also evaluated heterogeneity variables on perfusion parameters and assessed the relationship between heterogeneity analysis results and histogram differences. The tumor uniformity of permeability increased on day 1 after irradiation and the percent change showed a significantly higher uniformity of permeability than nonirradiated tumors on day 1 after irradiation, which was corroborated by a previous study by Goh et al. (23), reflecting reduced tumor heterogeneity.

The situation was the same for entropy values of both BV and permeability. We found a consistent tendency of decreased entropy values after treatment. Even though those changes failed to reach statistical significance, it could be because of the sample size. These results would be consistent with a decrease in vascularization and the development of necrosis. This is also supported by findings of prior studies, which have suggested that texture reflects the underlying vascularization (34).

There were limitations to this study. CT measurements of permeability reflect a complex interaction between microvascular environments such as capillary surface area, interstitial pressure, perfusion, and pore size. Additionally, the generalized applicability of our results might potentially be limited by the insufficient sample size. We evaluated whole tumor cell apoptosis to assess therapeutic efficacy rather than the microvascular effects of radiotherapy, which can be assessed by endothelial apoptosis.

In conclusion, our observations demonstrate that the histogram analysis of CT perfusion parameters has the potential to provide predictive information for treatment response to radiotherapy. However, this remains to be validated in a larger prospective series, and the extension of the analysis to other clinical imaging modalities could be feasible, thus providing for a possible unified analytical approach for quantitative image analysis for the early prediction of tumor therapeutic response.

Conflict of interest disclosure

The authors declared no conflicts of interest.

Financial disclosure

This research was supported by Basic Science Research Program through the National Research Foundation of Korea (NRF) funded by the Ministry of Education (NRF-2013R1A1A2063746).

References

1. Grothey A, Hedrick EE, Mass RD, et al. Response-independent survival benefit in metastatic colorectal cancer: a comparative analysis of N9741 and AVF2107. J Clin Oncol 2008; 26:183–189. [CrossRef]
2. Sathornsumetee S, Cao Y, Marcello JE, et al. Tumor angiogenic and hypoxic profiles predict radiographic response and survival in malignant astrocytoma patients treated with bevacizumab and irinotecan. J Clin Oncol 2008; 26:271–278. [CrossRef]
3. Goh V, Halligan S, Daley F, Wellsted DM, Guenther T, Bartram CI. Colorectal tumor vascularity: quantitative assessment with multidetector CT--do tumor perfusion measurements reflect angiogenesis? Radiology 2008; 249:510–517. [CrossRef]
4. Goldmacher GV, Conklin J. The use of tumour volumetrics to assess response to therapy in anticancer clinical trials. Br J Clin Pharmacol 2012; 73:846–854. [CrossRef]
5. Herbst RS, Onn A, Sandler A. Angiogenesis and lung cancer: prognostic and therapeutic implications. J Clin Oncol 2005; 23:3243–3256. [CrossRef]
6. Garcia-Barros M, Paris F, Cordon-Cardo C, et al. Tumor response to radiotherapy regulated by endothelial cell apoptosis. Science 2003; 300:1155–1159. [CrossRef]
7. Ng QS, Goh V, Milner J, Padhani AR, Saunders MI, Hoskin PJ. Acute tumor vascular effects following fractionated radiotherapy in human lung cancer: In vivo whole tumor assessment using volumetric perfusion computed tomography. Int J Radiat Oncol Biol Phys 2007; 67:417–424. [CrossRef]
8. Thomlinson RH, Gray LH. The histological structure of some human lung cancers and the possible implications for radiotherapy. Br J Cancer 1955; 9:539–549. [CrossRef]
9. Kan Z, Phongkitkarun S, Kobayashi S, et al. Functional CT for quantifying tumor perfusion in antiangiogenic therapy in a rat model. Radiology 2005; 237:151–158. [CrossRef]
10. Cenic A, Nabavi DG, Craen RA, Gelb AW, Lee TY. A CT method to measure hemodynamics in brain tumors: validation and application of cerebral blood flow maps. AJNR Am J Neuroradiol 2000; 21:462–470.
11. Griffith B, Jain R. Perfusion imaging in neuro-oncology: basic techniques and clinical applications. Radiol Clin North Am 2015; 53:497–511. [CrossRef]

12. Kambadakone A, Yoon SS, Kim TM, et al. CT perfusion as an imaging biomarker in monitoring response to neoadjuvant bevacizumab and radiation in soft-tissue sarcomas: comparison with tumor morphology, circulating and tumor biomarkers, and gene expression. AJR Am J Roentgenol 2015; 204:W11–18. [CrossRef]
13. Miles KA, Charnsangavej C, Lee FT, Fishman EK, Horton K, Lee TY. Application of CT in the investigation of angiogenesis in oncology. Acad Radiol 2000; 7:840–850. [CrossRef]
14. Prezzi D, Khan A, Goh V. Perfusion CT imaging of treatment response in oncology. Eur J Radiol 2015; 84:2380–2385. [CrossRef]
15. Kambadakone AR, Sahani DV. Body perfusion CT: technique, clinical applications, and advances. Radiol Clin North Am 2009; 47:161–178. [CrossRef]
16. Galban CJ, Chenevert TL, Meyer CR, et al. The parametric response map is an imaging biomarker for early cancer treatment outcome. Nat Med 2009; 15:572–576. [CrossRef]
17. Freiman M, Voss S, Warfield SK. NdH/dT: A new quantitative measure for Diffusion Weighted Imaging based evaluation of abdominal tumor response to therapy. Proc Intl Soc Mag Reson Med 2011;19:838. Available: http://cds.ismrm.org/protected/811MProceedings/files/838.pdf.
18. Neri A, Welch D, Kawaguchi T, Nicolson GL. Development and biologic properties of malignant cell sublines and clones of a spontaneously metastasizing rat mammary adenocarcinoma. J Natl Cancer Inst 1982; 68:507–517.
19. Park CM, Goo JM, Lee HJ, et al. FN13762 murine breast cancer: region-by-region correlation of first-pass perfusion CT indexes with histologic vascular parameters. Radiology 2009; 251:721–730. [CrossRef]
20. Ng QS, Goh V, Fichte H, et al. Lung cancer perfusion at multi-detector row CT: reproducibility of whole tumor quantitative measurements. Radiology 2006; 239:547–553. [CrossRef]
21. Schwickert HC, Stiskal M, Roberts TP, et al. Contrast-enhanced MR imaging assessment of tumor capillary permeability: effect of irradiation on delivery of chemotherapy. Radiology 1996; 198:893–898. [CrossRef]
22. Patlak CS, Blasberg RG, Fenstermacher JD. Graphical evaluation of blood-to-brain transfer constants from multiple-time uptake data. J Cereb Blood Flow Metab 1983; 3:1–7. [CrossRef]
23. Goh V, Ganeshan B, Nathan P, Juttla JK, Vinayan A, Miles KA. Assessment of response to tyrosine kinase inhibitors in metastatic renal cell cancer: CT texture as a predictive biomarker. Radiology 2011; 261:165–171. [CrossRef]
24. Ganeshan B, Miles KA, Young RC, Chatwin CR. Hepatic entropy and uniformity: additional parameters that can potentially increase the effectiveness of contrast enhancement during abdominal CT. Clin Radiol 2007; 62:761–768. [CrossRef]
25. Beasley MB, Brambilla E, Travis WD. The 2004 World Health Organization classification of lung tumors. Semin Roentgenol 2005; 40:90–97. [CrossRef]
26. Kim H, Morgan DE, Zeng H, et al. Breast tumor xenografts: diffusion-weighted MR imaging to assess early therapy with novel apoptosis-inducing anti-DR5 antibody. Radiology 2008; 248:844–851. [CrossRef]
27. Haralick RM, Sternberg SR, Zhuang X. Image analysis using mathematical morphology. IEEE Trans Pattern Anal Mach Intell 1987; 9:532–550. [CrossRef]
28. Goh V, Halligan S, Bartram CI. Quantitative tumor perfusion assessment with multidetector CT: are measurements from two commercial software packages interchangeable? Radiology 2007; 242:777–782. [CrossRef]
29. Ng QS, Goh V, Klotz E, et al. Quantitative assessment of lung cancer perfusion using MDCT: does measurement reproducibility improve with greater tumor volume coverage? AJR Am J Roentgenol 2006; 187:1079–1084. [CrossRef]
30. Moeller BJ, Cao Y, Li CY, Dewhirst MW. Radiation activates HIF-1 to regulate vascular radiosensitivity in tumors: role of reoxygenation, free radicals, and stress granules. Cancer Cell 2004; 5:429–441. [CrossRef]
31. Reiner CS, Goetti R, Eberli D, et al. CT perfusion of renal cell carcinoma: impact of volume coverage on quantitative analysis. Invest Radiol 2012; 47:33–40. [CrossRef]
32. de Vries A, Griebel J, Kremser C, et al. Monitoring of tumor microcirculation during fractionated radiation therapy in patients with rectal carcinoma: preliminary results and implications for therapy. Radiology 2000; 217:385–391. [CrossRef]
33. Sahani DV, Kalva SP, Hamberg LM, et al. Assessing tumor perfusion and treatment response in rectal cancer with multisection CT: initial observations. Radiology 2005; 234:785–792. [CrossRef]
34. Bezy-Wendling J, Kretowski M, Rolland Y, Le Bidon W. Toward a better understanding of texture in vascular CT scan simulated images. IEEE Trans Biomed Eng 2001; 48:120–124. [CrossRef]